Discovery of an Isothiazolinone-Containing Antitubercular Natural Product Levesquamide

Libang Liang[†], Bradley Haltli[‡,§], Douglas H. Marchbank[†,§], Maike Fischer[⌋], Christopher W. Kirby[†,⌋], Hebelin Correa[§], Trevor N. Clark[‖], Christopher A. Gray[‖,^], Russell G. Kerr[*,†,‡,§]

[†]Department of Chemistry and [‡]Department of Biomedical Sciences, University of Prince Edward Island, 550 University Avenue, Charlottetown, PE C1A 4P3, Canada

[§]Nautilus Biosciences Croda, 550 University Avenue, Regis and Joan Duffy Research Centre, Charlottetown, PE C1A 4P3, Canada

[⌋]Charlottetown Research & Development Centre, Agriculture and Agri-Food Canada, 440 University Avenue, Charlottetown, PE C1A 4N6, Canada

[‖]Department of Chemistry, University of New Brunswick, 30 Dineen Drive, Fredericton, NB E3B 5A3, Canada

[^]Department of Biological Sciences, University of New Brunswick, 100 Tucker Park Road, Saint John, NB E2L 4L5, Canada

*Corresponding Author

ABSTRACT

Antitubercular agent levesquamide is a new polyketide-nonribosomal peptide (PK-NRP) hybrid marine natural product isolated from *Streptomyces* sp. RKND-216. The structure contains a rare isothiazolinone moiety which has only been reported in collismycin SN. Structure elucidation by NMR spectroscopy was a significant challenge due to a deficiency of protons in this aromatic moiety. Therefore, the genome of *Streptomyces* sp. RKND-216 was sequenced to identify the levesquamide biosynthetic gene cluster (BGC). Analysis of the BGC provided structural insights and guided stable-isotope labeling experiments, which led to the assignment of the fused pyridine-isothiazolinone moiety. The BGC and the labeling experiments provide further insights into the biosynthetic origin of isothiazolinones. Levesquamide exhibited antimicrobial activity in the microplate alamarBlue assay (MABA) and low oxygen recovery assay (LORA) against *Mycobacterium tuberculosis* H37Rv with minimum inhibitory concentration (MIC) values of 9.65 and 22.28 μM, respectively. Similar activity was exhibited against rifampicin- and isoniazid-resistant *M. tuberculosis* strains with MIC values of 9.46 and 9.90 μM, respectively. This result suggests levesquamide has a different mode of action against *M. tuberculosis* compared to the two first-line antitubercular drugs rifampicin and isoniazid. Furthermore, levesquamide shows no cytotoxicity against the Vero cell line, suggesting it may have a useful therapeutic window.

INTRODUCTION

Only about 100 natural products are known to contain a sulfur-nitrogen bond,[1] among which isothiazoles are uncommon while isothiazolinones are extremely rare. Isothiazoles brassilexin[2] and sinalexin[3], isolated from the plants *Brassica juncea* and *Sinapis alba*, respectively, are known to be two of the most potent phytoalexins produced by cruciferous plants (Figure 1). Aulosirazole is a cytotoxic natural product isolated from blue-green algae with selective inhibitory activities against solid tumor cells.[4] Pronqodine A was isolated from *Streptomyces* sp. MK832-95F2 which inhibited cyclooxygenase enzyme activity in the presence of NAD(P)H dehydrogenase quinone 1 (NQO1).[5] *Streptomyces* species are also the source of the collismycins,[6] which are known to exhibit a wide range of biological activities, including antibacterial, antifungal, cytotoxic,[7] anti-inflammatory,[8] and neuro-protective activities.[9] The biosynthetic gene cluster (BGC) of collismycin A was recently identified from *Streptomyces* sp. CS40 and contains 27 genes.[6(b)] In this study, a biosynthetic intermediate collismycin SN, which contains an uncommon isothiazolinone moiety, was isolated from a methyltransferase (*clmM1*) mutant.

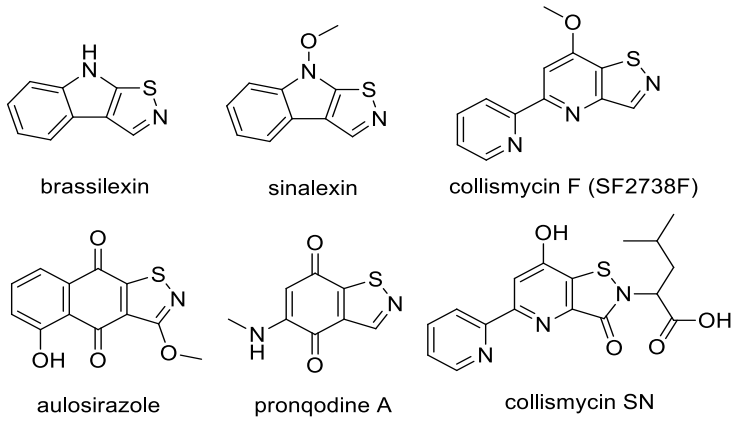

Figure 1. Natural products containing an isothiazole or an isothiazolinone moiety.

Despite the interesting biological activities of these natural products, little is known about the biosynthesis of isothiazole or isothiazolinone moieties. Although the BGC of collismycin A is now available, it is not clear which of the 27 genes is involved in the formation of the isothiazolinone moiety of collismycin SN. Structurally similar to the collismycins, caerulomycins share a 2,2'- bipyridine core structure but lacks the sulfur substitution on one of the pyridine rings.[10] A comparative study of the BGCs between caerulomycins and collismycins suggested they have a common biosynthetic pathway involving an intramolecular cyclization and rearrangement of a sulfur-containing seven-member ring.[11] A subsequent 2,3-dehydrogenation generates collismycins while 2,5-desulfurization produces caerulomycins,[11] providing insights for the biosynthesis of collismycin SN.

We report herein the isolation and structural characterization of levesquamide (**1**), an isothiazolinone-containing natural product. Stable-isotope labeling confirmed the presence of a pyridine ring, which originates from an unusual linkage between malonate and cysteine moieties, consistent with previous labeling studies that established the biosynthesis of the 2,2'-bipyridine ring of collismycins and caerulomycins.[11] We identified the putative levesquamide BGC using AntiSMASH5.0.0 and established its involvement in levesquamide biosynthesis via gene inactivation and complementation experiments.[12] Further, we describe a comparative analysis of the levesquamide and collismycin A BGCs to shed further light into the mechanism of nitrogen-sulfur bond formation in these isothiazolinone-containing natural products.

RESULTS AND DISCUSSION

Isolation and Partial Structural Characterization of Levesquamide (1). Levesquamide (**1**) was isolated from 6 L of *Streptomyces* sp. RKND-216 fermentation broth. High-resolution mass spectrometry (HRMS) analysis of **1** showed a protonated ion of *m/z* 631.2180 $[M+H]^+$ (Figure S1), indicating a molecular formula of $C_{28}H_{34}O_9N_6S$ and 15 degrees of unsaturation. Initially, partial structures of **1** were elucidated using one- and two-dimensional NMR techniques (Table 1). In the ^{1}H NMR spectrum, a spin system consisting of four aryl protons H-A4 (δ_H 6.87), H-A5 (δ_H 7.22), H-A6 (δ_H 6.63) and H-A7 (δ_H 7.75) were established through COSY correlations. HMBC correlations from H-A4 and H-A6 to C-A2 (δ_C 106.6) as well as from H-A5 and H-A7 to C-A3 (δ_C 147.7) indicated the presence of an *ortho*-disubstituted benzene moiety (Figure 2).

Proton signal NH_2-A3 (δ_H 7.00 ppm) integrated to two protons and showed a ^{1}H-^{15}N HSQC correlation with a ^{15}N resonance at 64.5 ppm, confirming the presence of a primary amino group. This proton signal also exhibited HMBC correlations with C-A4 (δ_C 116.0) and C-A2, suggesting the primary amino group was attached to position C-A3. Proton resonance H-A7 showed a HMBC correlation with carbon C-A1 (δ_C 160.6), indicating the presence of an anthranilate moiety.

In the HMBC spectrum, aryl proton resonance H-^{1}S3 (δ_H 8.75) also showed a correlation with C-A1, in addition to another correlation with C-^{1}S2 (δ_C 131.2). Comparison of these chemical shift values with those reported for oxazole and thiazole moieties suggested these signals belonged to an oxazole ring attached to the anthranilate moiety.[13] However, no ^{1}H-^{15}N HMBC correlation was observed between H-^{1}S3 and the oxazole nitrogen. A stable isotope labeling experiment using [^{15}N]-NH_4Cl resulted in the incorporation of ^{15}N, as indicated by UHPLC-HRMS analysis (Figure S1), and enhancement of the ^{1}H-^{15}N HMBC correlation between H-^{1}S3 and N-^{1}S2 (Figure S10). Oxazole proton resonance H-^{1}S3 also exhibited HMBC correlations with C-^{1}S1 (δ_C 158.4), and C-Ac2 (δ_C 145.1). In the HMBC spectrum, methyl resonance MeO-Ac2 (δ_H 3.97 ppm) showed a correlation with C-Ac2 as well, suggesting a methoxy substituent was located at position C-Ac2. In a selective 1D ROESY experiment, irradiation of H-^{1}S3 enhanced the methoxy proton signal (Figure S11), which indicated the spatial proximity between these two protons and led to the assignment of partial structure A (Figure 2).

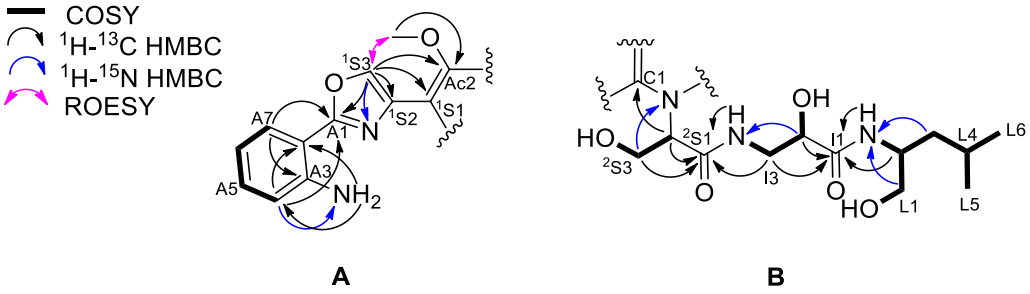

Figure 2. Partial structures **A** and **B** elucidated from preliminary NMR experiments.

Meanwhile, partial structure B was elucidated as a tripeptide moiety consisting of leucinol, isoserine, and serine residues. The isopropyl group of leucinol was identified by two methyl proton signals H-L5 (δ_H 0.86) and H-L6 (δ_H 0.83), which showed COSY correlations with methine proton H-L4 (δ_H 1.55). The remaining spin system of leucinol was established by further analysis of COSY correlations. Methine proton H-L2 (δ_H 3.81) and amide proton resonance NH-L2 (δ_H 7.38) each exhibited HMBC correlations with carbonyl carbon C-I1 (δ_C 171.4). An isoserine moiety was established by interpreting COSY correlations from methine H-I2 (δ_H 3.97) to methylene protons H-I3a (δ_H 3.46)/H-I3b (δ_H 3.12) and hydroxyl proton OH-I2 (δ_H 5.74 ppm). Amide proton NH-I3(δ_H 8.43) also showed a COSY correlation with methylene proton H-I3. HMBC correlations from H-I2, H-I3a/H-I3b and H-L2 to C-I1 indicated that the isoserine and leucinol residues were attached through an amide bond. The remaining amino acid residue of the tripeptide moiety was confirmed to be serine by COSY correlations from methylene proton resonance H-^{2}S3 (δ_H 3.81) to methine H-^{2}S2 (δ_H 5.32) and OH-^{2}S3 (δ_H 3.81). HMBC correlations

between protons H-^{2}S2, H-^{2}S3 and H-I3 and carbonyl resonance C-^{2}S1 (δ_C 167.6) established the connectivity between the serine and isoserine residues. Nitrogen resonance N-^{2}S2 at (δ_N 125.6) belonging to the serine moiety was observed through an HMBC correlation with methylene proton H-^{2}S3. Serine nitrogen N-^{2}S2 was determined to be fully substituted as no other amide proton signals were observed. Methine proton H-^{2}S2 showed an HMBC correlation to carbonyl resonance C-C1 (δ_C 166.1), which therefore belonged to the amide functionality consisting of serine nitrogen N-^{2}S2. No other correlations were observed in the HMBC spectrum to establish the chemical structure beyond the carbonyl carbon C-C1.

Table 1. NMR spectroscopic data (600 MHz, DMSO-d_6) for levesquamide (**1**).

	position	$\delta_{C/N}$, type	δ_H, mult. (J in Hz)	COSY[a]	HMBC[a]
Anthranilate	A1	160.6, C	-	-	-
	A2	106.6, C	-		-
	A3	147.7, C	-	-	-
	A4	116.0, CH	6.87, dd (0.8, 8.4)	A5	A6, A2, A1, A3-NH_2
	A5	131.8, CH	7.22, ddd (6.9, 8.4, 1.3)	A4, A6	A3, A7
	A6	115.0, CH	6.63, dd (7.8, 6.9)	A5, A7	A4, A5, A2, A7
	A7	127.3, CH	7.75, dd (0.8, 7.8)	A6	A3, A5, A1
	NH_2-A3	64.5[b], NH_2	7.00, s	-	A4
[1]Serine	[1]S1	158.4[c], C	-	-	-
	[1]S2	131.2[e], C	-		-
	[1]S3	139.9[e], CH	8.75[e], s	-	A1, [1]S2, [1]S1, [1]S2-N
	N-[1]S2	236.4[b], N	-	-	-
Acetate	Ac1	162.4[d], C	-	-	-
	Ac2	145.1[d], C	-	-	-
	OH-Ac1	-	nd	-	-
	MeO-Ac2	58.7, CH_3	3.97, s	-	Ac2
Cysteine	C1	166.1[d], C	-	-	-
	C2	134.9[d], C	-	-	-
	C3	132.0[d], C	-	-	-
	N-C2	nd	-	-	-
[2]Serine	[2]S1	167.6, C	-	-	-
	[2]S2	58.5, CH	5.32, t (5.5)	[2]S3	C2[c], C1, [2]S3
	[2]S3	61.6, CH_2	3.81, m	[2]S2, [2]S3-OH	[2]S2, [2]S1
	OH-[2]S3	-	5.32, broad	[2]S3	-
	N-[2]S2	125.6[b], N	-	-	-
Isoserine	I1	171.4, C	-	-	-
	I2	70.1, CH	3.97, m	I3, I2-OH	I3, I1
	I3a	43.4, CH_2	3.46, m	I2, I3b, I3-NH	[2]S1, I2, I1
	I3b		3.12, m	I2, I3a, I3-NH	
	OH-I2	-	5.74, d (5.1)	I2	I3, I2, I1

	NH-I3	111.6[b], NH	8.43, t (5.7)	I3	I3, ^{2}S2, I2, ^{2}S1
Leucinol	L1a	63.6, CH_2	3.35, m	L1b, L2, L1-OH	L3, L2
	L1b		3.28, m	L1a, L2, L1-OH	
	L2	48.4, CH	3.81, m	L1, L3, L2-NH	L4, L1, L3, I1
	L3	40.1, CH_2	1.31, m	L2, L4	L2, L4, L5, L6, L1
	L4	24.2, CH	1.55, m	L3, L5, L6	L2, L3, L5, L6
	L5	23.3, CH_3	0.86, d (6.7)	L4	L6, L3
	L6	22.0, CH_3	0.83, d (6.5)	L4	L5, L3
	OH-L1	-	4.67, s	L1	-
	NH-L2	121.5[b], NH	7.38, d (9.14)	L2	L3, L2, L1, I2, I1

[a] COSY and HMBC correlations are from proton(s) stated to the indicated proton, carbon (coupling optimized for J = 5 Hz) or nitrogen (coupling optimized for J = 5 Hz); [b] ^{15}N chemical shift values obtained from ^{1}H-^{15}N HMBC experiment (400 MHz, CD_3OD) using ^{15}N-labeled **1** and calibrated by indirect referencing[14] to ammonia. [c] ^{13}C chemical shift values recorded from ^{1}H-^{13}C HMBC experiments (400 MHz, DMSO-d_6) with coupling optimized for J = 1 Hz; [d] Signals measured from ^{13}C stable isotope-labeled **1**; [e] chemical shifts varied in a different sample, $\delta_C{}^{1}{}_{S2}$ 139.3, $\delta_H{}^{1}{}_{S3}$ 8.35, $\delta_C{}^{1}{}_{S3}$ 137.1; nd: not determined.

Given the peptidyl backbone in partial structures A and B, levesquamide (**1**) appeared to be a linear nonribosomal peptide (NRP) with an anthranilate-oxazole and a tripeptide moiety flanking an unknown region of the structure. Based on the molecular formula, one proton and three carbons remained to be assigned, although these were not observed in the ^{1}H and ^{13}C NMR spectra. Notably, non-protonated carbon resonances including C-^{1}S1 and C-^{1}S2 were only detected in the HMBC spectrum as they showed weak signal-to-noise in the ^{13}C spectrum, possibly a result of long relaxation times and/or signal broadening. Efforts to elucidate the remaining portion of **1** (C_3HNO_2S) by increasing the relaxation delay (d1) for ^{13}C spectra acquisition, investigating fragment ions by tandem mass spectrometry (Figure S2), and forming crystals for X-ray crystallography studies were unsuccessful.

Identification of the levesquamide (1) biosynthetic gene cluster. To gain further insights into the structure of **1**, the genome of *Streptomyces* sp. RKND-216 was sequenced and annotated using the Prokaryotic Genome Annotation Pipeline (version 4.8)[15], while antiSMASH 5.0.0[16] and PRISM4[17] were used to identify the BGC of **1**.[18] Both programs identified eighteen putative BGCs (14 BGCs in common), ten of which contained nonribosomal peptide synthetases (NRPSs), which we predicted would be required for levesquamide biosynthesis. BGC1 contained NRPSs with predicted adenylation (A) domain substrate specificities consistent with the levesquamide partial structure (Figure 2). BGC1 (genome location: 243,396 bp - 311,170 bp) encoded a hybrid NRPS-PKS BGC spanning 67,775 bp, consisting of 48 open reading frames (ORFs) (Figure 3A; Table S1).

BGC1 contained four large genes encoding three NRPSs and one mixed NRPS/PKS. Examination of the domain organization identified LvqA as the first NRPS in levesquamide-biosynthesis. LvqA consists of a loading module containing a CoA-ligase (CAL) and thiolation (T) domain and an extension module with the domain organization: cyclization (Cy) - adenylation (A) - oxidase (Ox) -T. The CAL domain was predicted to activate a long-chain fatty acid or to be involved in *β*-aminoalaninamide biosynthesis, analogous to the function of the CAL domain in the bleomycin NRPS loading module.[19] These predictions were inconsistent with the partial levesquamide structure which indicated anthranilate was the starting unit (Figure 2). Comparison of the CAL domain's 10 amino acid (aa) substrate specificity code[20] to those from the bleomycin CAL domain and several fatty acid- or aryl acid-activating CAL and A domains indicated that the specificity code of the LvqA CAL domain was most similar to those of established anthranilate activating enzymes PqsA[21] and anaPS-A1[22] (Table S2). In addition, LvqN encodes a tryptophan 2,3-dioxygenase (56% identity; 69% similarity; accession no. TMD29316.1) which may participate in anthranilate supply. This data suggests module 1 loads anthranilate as the starting unit, which is consistent with partial structure A (Figure 2). The predicted substrate of the module 2 A domain was Cys, however, the specificity code did not closely match the consensus specificity codes for either Cys or Ser (Table S3). Based on partial structure A in Figure 2, we propose that the A domain activates Ser, which is subsequently condensed with anthranilate and cyclized and dehydrated to form an oxazoline ring by the Cy domain. The partial levesquamide structure indicated that the oxazoline ring formed by the Cy domain was oxidized to the more stable oxazole. Oxazoline oxidation is typically catalyzed by Ox domains.[23] An Ox domain was not detected by antiSMASH, while PRISM4 predicted the presence of a nitroreductase domain between the A and T domains. Blastp analysis of this region identified a McbC-like oxidoreductase domain between residues 1719 and 1897 of LvqA (E-

value 4.24e^{-38}). This protein family encompasses NRPS oxidase domains. Further analysis of the domain with the NCBI conserved domain database (CDD)[24] revealed that the conserved flavin mononucleotide and NADPH binding site residues were intact, suggesting that the oxidase domain is active, which is consistent with the presence of an oxazole ring in the levesquamide structure.

Downstream from *lvqA* is an apparent operon of three NRPS/PKS genes, *lvqB-D.* The stop codon of *lvqB* overlaps the start condon of *lvqC* by four bp, while *lvqC* is followed closely (1 bp) by *lvqD*, suggesting these genes may be translationally coupled.[25] LvqB consists of a PKS (module 3, KS-AT-T) and NRPS module (module 4, Cy-A-T-E*). Malonyl-CoA was the predicted substrate of module 3 AT, suggesting module 3 catalyzes the addition of an acetate. The module 4 A domain was predicted to activate Cys (Table S3) and the presence of a Cy domain suggested this module may form a thiazoline ring. PRISM4 predicted the presence of an E domain at the end of LvqB, which was not predicted by antiSMASH. Comparison of this domain to the E-domains of tyrocidine synthetase 1 (accession no. AAC45928) and gramicidin synthetase 1 (accession no. P0C061) revealed that the module 4 E domain was likely inactive as it lacked the essential catalytic His residue in the E2 conserved domain (HELLVDG *vs.* HHxxxDG) and the essential Tyr residue in the E7 domain (VRHLGA *vs.* FNYLGQ).[26]

Colinear incorporation of an acetate and thiazole ring following the oxazole generated by LvqA was not consistent with partial structures A and B, which we were unable to connect due to a high degree of aromaticity between these moieties. This suggested the acetate and cysteine incorporated by LvqB were modified in an unanticipated manner to generate a highly aromatic ring system. This prompted us to investigate LvqB further. Interestingly, this protein exhibited a high degree of homology to ClmN1 and CaeA2 (50% identity and > 60% similarity) from the collismycin[6(b)] and caerulomycin[11] BGCs, respectively. These enzymes incorporate acetate and cysteine to form the second pyridine ring in the 2,2'-bipyridine core common to collismycin and caerulomycins.[6(b)] Garcia and co-workers demonstrated that insertional inactivation of the sulphur methyltransferase, ClmM1, abolished collismycin biosynthesis and led to the production of collismycin SN containing an isothiazolinone moiety fused to the second pyridine ring (Figure 3). A ClmM1 homolog was not present in the levesquamide BGC, leading us to predict a similar cyclization may occur in levesquamide biosynthesis, forming a fused pyridine-isothiazolinone bicyclic ring system linking partial structures A and B (Figure 3B). The prevalence of non-protonated carbons and the paucity of protons in this region would explain our inability to establish HMBC correlations linking the partial structures.

LvqC encoded a single NRPS module (module 5) with a C-A-T domain organization. Analysis of module 5 A domain using NPRSPredictor2[27] predicted Thr (small clusters prediction) and Ser (large clusters prediction) as likely substrates. In keeping with this prediction, the extracted 10 aa specificity code was an imperfect match to both the Ser and Thr consensus specificity codes (Table S3). Based on partial structure B (Figure 2), we propose module 5 incorporates a Ser residue following the isothiazolinone ring. LvqD encoded modules 6 and 7 with the domain organization C-A-T-C-A-T-Re. The predicted module 6 A domain substrate was Gly, however, the partial structure B indicated isoserine (isoSer) was likely incorporated by this module. To the best of our knowledge isoSer has been identified as a component of only three natural products: edeine[28], theopalauamide[29] and theonellamides[30]. In theonellamide biosynthesis, module 3 of the NRPS TnaP contains an A domain that is predicted to activate *β*-alanine (*β*-Ala). The *β*-Ala residue is subsequently hydroxylated to form isoSer, although the hydroxylation enzyme was not

identified.[30] Comparison of the LvqD module 6 A-domain specificity codes to other *β*-Ala-activating A domains (including, TnaP module 3) revealed very little similarity (Table S3). We next scanned the levesquamide BGC for enzymes involved in *β*-Ala biosynthesis and discovered an L-aspartate-1-decarboxylase (LvqG) which exhibited strong homology to KirD (accession no. CAN89641.1; 43% identity; 57%; similarity) from the *Streptomyces collinus* Tü 365 kirromycin BGC.[31] In kirromycin biosynthesis KirD decarboxylates L-aspartate to generate *β*-Ala, which is incorporated into kirromycin peptide by the NRPS KirB (accession no. CAN89638.1). This prompted us to examine the substrate prediction for the proven *β*-Ala-activating KirB[31] A domain. AntiSMASH and PRISM4 predicted Gly as the substrate of the KirB A domain. Comparison of the A-domain specificity codes from Gly, KirB and LvqD *β*-Ala-activating A-domains revealed they were strikingly similar (Table S3). This similarity is not surprising given the chemical structure of *β*-Ala has only one additional methylene group compared to Gly. The similarity between kirromycin and levesquamide biosynthetic enzymes suggests LvqG likely generates *β*-Ala which is then activated by the module 6 A domain for peptide chain extension. IsoSer could then be generated by hydroxylation of the *β*-Ala residue similar to theonellamides[30].

The terminal module of LvqD of module 7 likely incorporates Leu based on an 80% match to the Stachelhaus specificity code (80% match),[20] which is consistent with partial structure B (Figure 2). A reductase (Re) domain was detected at the carboxyl-terminus of LvqD. Re-domains utilize NAD(P)H as a co-factor to reductively release T-bound intermediates as an aldehyde or alcohol.[32] The presence of a leucinol residue at the carboxy-terminus of levesquamide is consistent with partial structure B (Figure 2) and the enzymatic release of a peptide intermediate by an R-domain. A type II thioesterase encoded by *lvqJ* was identified downstream from *lvqD*. Type II thioesterases are frequently encountered in NRPS and PKS BGCs and have been proposed to remove aberrantly loaded substrates from T-domains to regenerate free thiols.[33]

In addition to the thiotemplate enzymes described for LvqA-D, antiSMASH and PRISM4 predicted *lvqE* encoded a stand-alone A domain. The CCD also suggested similarity between LvqE and AMP-binding super family proteins (E-value 2.10^{-7}, accession no. cl37995), however, the high E-value suggested poor confidence level of the prediction. Also, the highly conserved motif A4 (Asp235) in A domains essential for stabilizing α-amino groups of substrates[20] is missing in LvqE (Table S3). Therefore, LvqE is unlikely to be an active A domain and its function remains unclear.

Twelve putative tailoring enzymes were identified in the core biosynthetic locus. Five genes were predicted to play a role in oxidation reactions required for the biosynthesis of **1**. The CCD identified a UbiH-like domain in LvqH and Blastp analysis showed it was similar to FAD-dependent oxidoreductases (37% identity; 53% similarity; accession no. RKS76991.1). LvqK is a cupin-like superfamily protein (71% identity; 82% similarity; accession no. SCK55914.1), and LvqQ exhibits strong similarity to VOC family proteins[34] (90% identity; 94% similarity; accession no. AXK32700.1). Flanking the NRPS core of the levesquamide BGC two oxidoreductases, LvqL and LvqM were identified, however their roles in the biosynthesis of **1** are unclear. The putative oxidases identified in the BGC are likely responsible for hydroxylation of the putative pyridine ring at the Ac2 carbon, hydroxylation of *β*-Ala to form isoSer, and potential thiol oxidation although the specific role of each remains to be experimentally determined. LvqR is homologous to an alkyl hydroperoxide reductase (78% identity; 87% similarity; accession no. OEV29300.1) reported in peroxide response mechanisms and restoration of its catalytic function requires thioredoxins.[35] LvqP is similar to a thiol-disulfide

isomerase/thioredoxin (42% identity; 57% similarity; accession no. RZU78976.1), typically catalyzing reduction of sulfenic acid to a thiol via a disulfide intermediate in proteins.[36] LvqS is homologous to a pyridine nucleotide-disulfide oxidoreductase (80% identity; 82% similarity; accession no. KUH35663.1), which has been reported to catalyze formation of disulfide bonds from thiols in NRPSs.[37] LvqR, LvqP, and LvqS may be involved in formation of the sulfenamide moiety and the isothiazolinone ring in **1**. LvqF was similar to several classes of 1 *S*-adenosylmethionine (SAM)-dependent methyltransferases (e.g. 76% identity; 88% similarity; accession no. SCK55890.1) and the only methyltransferase in the BGC. Accordingly, LvqF was predicted to catalyze the methylation of the Ac2 hydroxy group. LvqO is adjacent to the LvqA NRPS and encodes a dTDP-glucose 4,6-dehydratase (42% identity; 56% coverage; accession no. HCU95362.1). These enzymes are typically associated with catalyzing the first dedicated step in deoxysugar biosynthesis.[38] Levesquamide is not glycosylated, nor are other sugar biosynthetic genes present in the BGC, thus the function of this enzyme is unknown. LvqI is similar to ClmD1 (51% identity; 64% similarity; accession no. CCC55923.1) a butyryl-CoA dehydrogenase proposed to be involved in the second pyridine ring formation in the collismycin A biosynthesis,[6(b)] and may play a role in pyridine ring formation in **1**.

Four transport-related genes were identified (*lvqT1* to *lvqT4*). LvqT1 and LvqT2 are sugar ATP-binding cassette proteins[39] that may facilitate carbohydrate uptake. LvqT3 (EmbR/QacA subfamily) and LvqT4 (major facilitator family) encode putative drug-resistance transporters[40] that may be involved in levesquamide transport and/or self-resistance. Six regulatory genes (*lvqR1-lvqR6*) and two TTA codons were identified in the BGC. The transcriptional regulators, *lvqR3* and *lvqR4,* are both homologous to NarL/FixJ family regulators and were identified flanking the core BGC region. Another regulatory gene, *lvqR2*, encoding a MurR/RpiR family regulator was found immediately upstream of *lvqR3*. The other three transcriptional regulator genes *lvqR1*, *lvqR5*, and *lvqR6* encode a ComR-like transcriptional repressor, a LuxR family transcriptional regulator, and a MarR family transcriptional regulator, respectively.

Validation of the levesquamide (1) BGC. To prove the involvement of BGC1 in levesquamide biosynthesis, mutant strains bearing a 339 bp in-frame deletion in *lvqF* were generated by homologous recombination. This mutation removed the SAM binding site in LvqF and was expected to abolish the methylating activity of the enzyme. Mutants were identified by PCR and the phenotype of the mutation was assessed by UHPLC-HRESIMS analysis of fermentation extracts from wild type (WT) and *lvqF* mutants. Production of **1** was essentially abolished in the *lvqF* mutants (Figure S18). Surprisingly, significant quantities of the expected desmethyl levesquamide analog were not produced in *lvqF* mutant fermentations. Complementation of mutants by ectopic expression of *lvqF* under control of the strong constitutive *ermE*p* promoter[41] restored production of **1** to 13.5% of WT levels. Conversely, complementation with the vector control did not restore production of **1** (Figure S18). Partial complementation of *lvqF* mutants, is likely due to altered expression levels or timing of expression from *ermE*p* as has been observed in other streptomycetes.[42] Detailed analysis of UHPLC-HRMS spectra of Δ*lvqF* mutant fermentation extracts identified trace levels of a desmethyl analog of **1** with a molecular formula of $C_{27}H_{32}O_9N_6S$ (m/z 617.2024 $[M+H]^+$) (Figure S19). This evidence, combined with results of the complementation experiment, unequivocally confirmed the involvement of BGC1 in the biosynthesis of **1**, and establish that *lvqF* is responsible for methylation in the biosynthesis of **1.** Interestingly, inactivation of LvqF resulted in a drastic reduction in the production level of

1, rather than formation of substantial quantities of the expected desmethyl analog. This suggests that the methylation performed by LvqF may occur early in the biosynthetic pathway, rather than as a post-NRPS tailoring step. Alternatively, inactivation of *lvqF* may have polar effects on downstream gene expression, resulting in low production of the desmethyl analog.

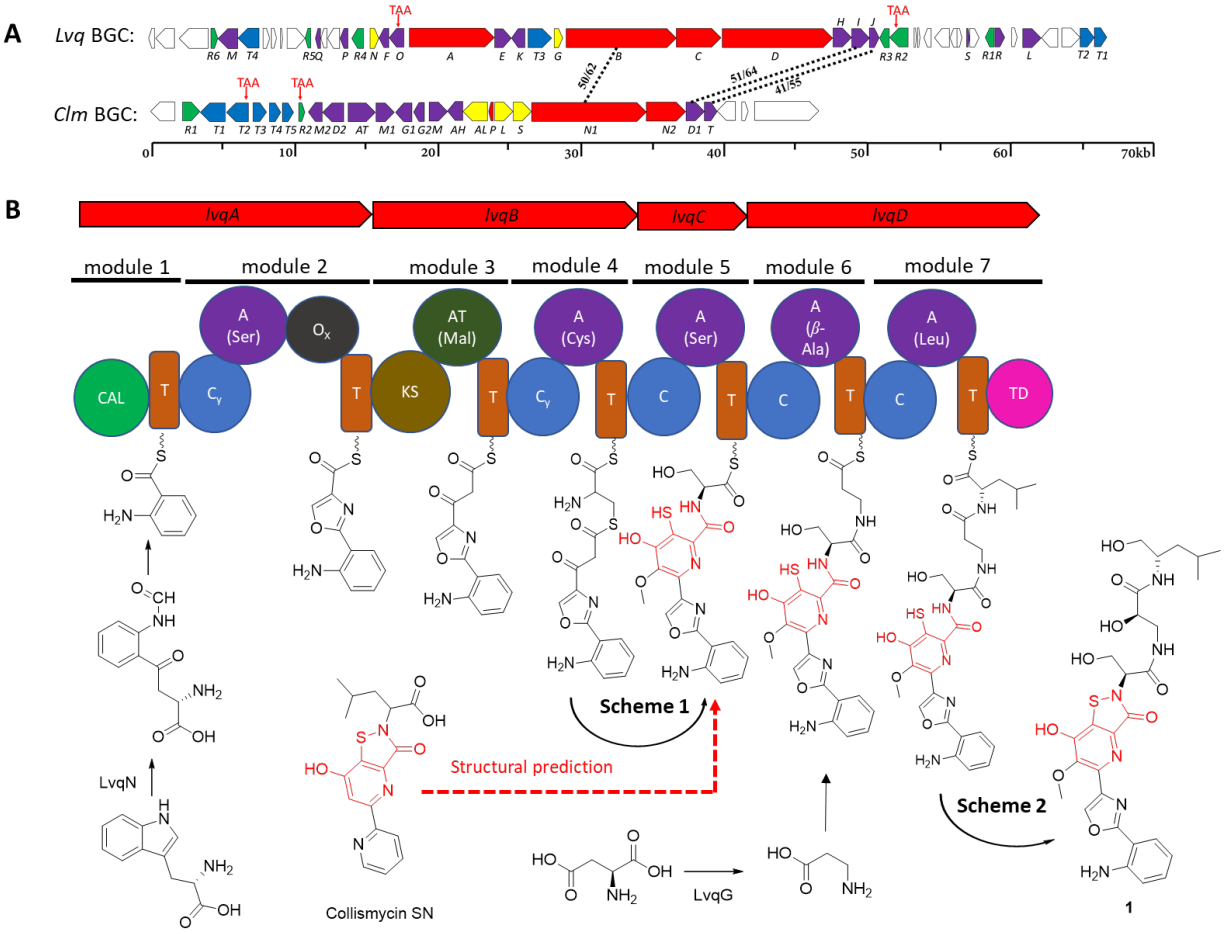

Figure 3. Levesquamide BGC. (A) Comparison of the levesquamide (*lvq*) and collisimycin (*col*) BGCs. Red: core biosynthetic genes; purple: additional biosynthetic genes; yellow: precursor supply genes; green: regulatory genes; blue: transport-related gees; white: genes with unknown functions. Locations of TAA codons are labeled. Dotted lines link homologous proteins from the two BGC (identity% / similarity%) (B) Proposed biosynthetic pathway of levesquamide. The partial structure highlighted in red was proposed based on the structural similarity to collismycin SN. Proposed biosynthetic pathways from modules 4 to 5 and after module 7 are described in Schemes 1 and 2.

Structural elucidation using stable isotope labeling. Inactivation of *lvqF* unambiguously established the role of BGC1 in levesquamide biosynthesis and bioinformatic analysis established a putative link between the biosynthesis of **1** and collismycin/caerulomycin biosynthesis, suggesting modules 3 and 4 function to generate a fused pyridine-isothioazolinone bicyclic ring system analogous to collismycin SN (Figure 3). We utilized the bioinformatic

analysis to guide a series of ^{13}C and ^{15}N stable-isotope labeling studies to unambiguously establish the structure of the proposed ring structure linking partial structures A and B.

To confirm the incorporation of malonate and cysteine units by module 3 and 4, sodium [1,2-$^{13}C_2$] acetate and L-[1,2,3-$^{13}C_3$, ^{15}N] cysteine were fed separately to fermentations of *Streptomyces* sp. RKND-216. From the [1,2-$^{13}C_2$] acetate labeling experiment, a protonated ion of *m/z* 633.2263 $[M+H]^+$ was observed by UHPLC-HRMS analysis (Figure S1), indicating that the label had been incorporated. Although the ^{13}C-UDEFT spectrum indicated that multiple positions were labeled, carbon resonances C-Ac2 and C-Ac1 (δ_C 162.4, d) were enhanced significantly and appeared as two doublets with identical coupling constants of 68 Hz, indicating that C-Ac2 is adjacent to C-Ac1 (Figure 4). Similarly, UHPLC-HRMS analysis confirmed the incorporation of L-[1,2,3-$^{13}C_3$, ^{15}N] cysteine, as indicated by a protonated ion of *m/z* 635.2248 $[M+H]^+$ (Figure S1). The ^{13}C-UDEFT spectrum[43] showed three carbon signals C-C1 (δ_C 166.1, app. dt), C-C2 (δ_C 134.9, ddd), C-C3 (δ_C 132.0, dd) that were significantly enhanced and *J*-coupled to one another (Figure 4A). This data provided the remaining carbon resonances and allowed their assignment to the 4-hydroxypyridine moiety of **1**. These observations also supported the predicted biosynthetic pathway in which malonate and cysteine were incorporated into **1** by *lvqB*. Notably, the L-[1,2,3-$^{13}C_3$, ^{15}N] cysteine labeled **1** suggested only one cysteine unit was incorporated by module 4, while none of the carbons incorporated by module 2 were affected, providing further evidence that module 2 incorporates Ser as opposed to Cys as predicted by antiSMASH and PRISM4.

To further confirm the proposed structure of **1** and establish the connectivity between C-Ac1 and C-C3, a feeding experiment using both sodium [1,2-$^{13}C_2$] acetate and L-[1,2,3-$^{13}C_3$, ^{15}N] cysteine was conducted to observe the $^1J_{CAc1\text{-}CC3}$ coupling. Based on UHPLC-HRMS analysis of the crude extract of this fermentation, a significant portion of **1** contained both labels as indicated by the presence of a mass peak with a *m/z* of 637.2327 $[M+H]^+$ (Figure S1). Given the presence of singly labeled **1**, resonances C-Ac1 and C-C3 were expected to be observed as a set of overlapping signals with different multiplicities. Resonances between C-Ac1 and C-C3 belonging to doubly labeled **1** were observed with a $^1J_{CAc1\text{-}CC3}$ coupling constant of 63 Hz (Figure 4 and Table 2), directly measured from C-Ac1, confirming the connectivity between the malonate and cysteine moieties in **1** and validating the BGC-predicted structure. Finally, the absolute configuration of the amino acid residues of the tripeptide chain was established as L-serine, D-isoserine, and L-leucinol by Marfey's analysis (Figure S15-S16). Observation of L-serine from Marfey's analysis also suggested the S-N bond in the cyclic sulfenamide moiety was hydrolyzed under acidic conditions releasing a free amide.

Table 2. Summary of ^{13}C-^{13}C coupling constants obtained from ^{13}C UDEFT NMR spectra (150 MHz, DMSO-d_6) of stable isotope labeled **1**.

	δ_C, mult. (J in Hz)		
	Acetate-labeled	Cysteine-labeled	Acetate/cysteine-labeled
C-C1	-	166.1, app. dt (80, 9)	166.1, app. dt (80, 9)
C-C2	-	134.9, ddd (80, 57, 4)	134.9, ddd (80, 57, 4)
C-C3	-	132.0, ddd (57, 9, 3)	132.0, m
C-Ac1	162.4, d (68)	-	162.4, dd (68, 63)
C-Ac2	145.1, d (68)	-	145.1, d (68)

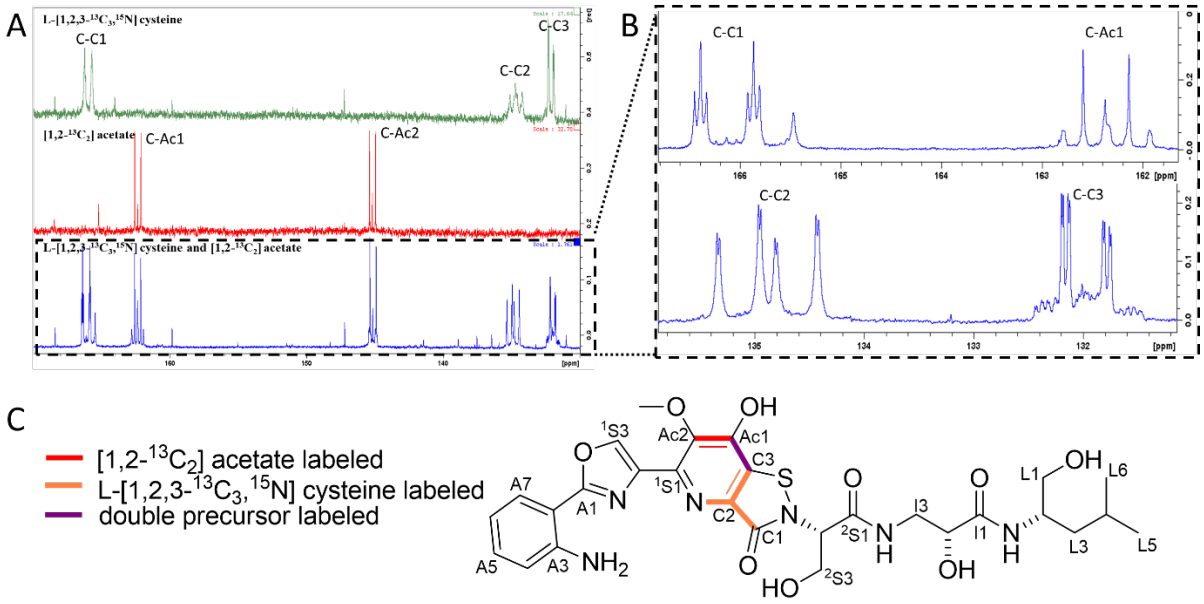

Figure 4. (A) Overlay of ^{13}C UDEFT spectra of levesquamide (**1**) from fermentations with [1,2-$^{13}C_2$] acetate, L-[1,2,3-$^{13}C_3$,^{15}N] cysteine and double feeding in DMSO-d_6. (B) Expanded spectrum of doubly labeled **1**. (C) Assignment of **1** showing bold bonds in red, orange and purple representing ^{13}C-^{13}C bonds established by coupling constant measurements.

Proposed biosynthetic pathway of levesquamide (1). Biosynthesis of levesquamide proceeds through a thiotemplate-directed process largely mediated by LvqA-D as described above. Having unambiguously established the structure of the central fused pyridine-isothiazolinone moiety of **1** we looked to collismycin[6(b),44] and caerulomycin[10(a),11, 45] biosynthesis for insights to how this moiety is formed. Following incorporation of the acetate extender unit by the PKS domain of module 3 we predict chain elongation by module 4 occurs between the sulfhydryl of cysteine and the carbonyl of the previously incorporated acetate unit derived from malonyl-CoA. Intramolecular cyclization of this intermediate would generate a seven-membered heterocycle,

which may undergo a rearrangement to release the thiol and generate a six membered ring common to collismycin and caerulomycin biosynthesis. Garcia and co-workers established that the acyl-CoA dehydrogenase encoded by *cmlD1* in the collismycin BGC was essential for collismycin A production in *Streptomyces* sp. CS40. Feeding collismycin SN to the Δ*clmD1* mutant resulted in conversion to collismycin A, suggesting *clmD1* catalyzed steps prior to formation of the isothiazole in collismycin A.[44] Additionally, Qu et al. proposed that the formation of the second pyridine ring in collismycins likely involves a 2,3-dehydrogenation step,[11] which was essential for the formation of collismycin SN. No other dehydrogenation step towards biosynthesis of collismycin SN would require an acyl-CoA dehydrogenase, thus ClmD1 probably catalyzes the 2,3-dehydrogenation step in collismycin SN biosynthesis. LvqI encodes an acyl-CoA dehydrogenase homologous to CmlD1 (51% identity, 64% similarity), which likely catalyzes the analogous dehydrogenation reaction from C-^{1}S1 and C-Ac2 in levesquamide biosynthesis (Scheme 1). Hydroxylation and O-methylation of the Ac2 carbon is required to complete the decoration of the pyridine ring. BGC1 contains four enzymes which may catalyze the hydroxylation step, LvqO, LvqM, LvqH and LvqK as described above. Methylation is catalyzed by LvqF as demonstrated by the aforementioned gene inactivation experiment.

Scheme 1. Proposed pyridine ring formation in levesquamide (1) biosynthesis.

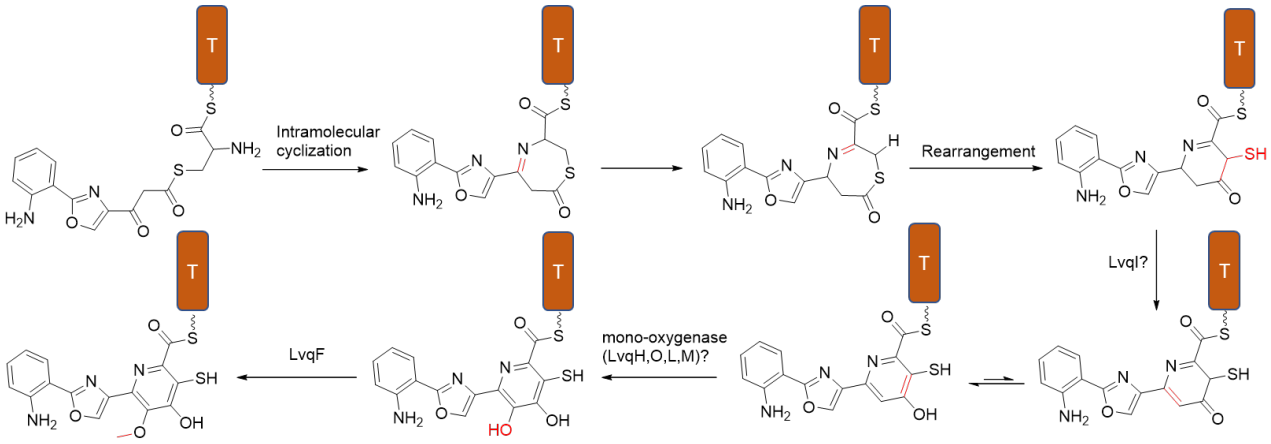

The biosynthesis of the isothiazolinone moiety is rare in natural products. However, formation of cyclic sulfenamide moieties has been well documented in bacterial and eukaryotic proteins undergoing oxidative stress,[46] although this functional group is rarely seen in small peptides. For example, when PTP1B is exposed to reactive oxygen species (ROS), catalytic cysteine residues Cys-215 is first oxidized to a sulfenic acid before intramolecular cyclization with the neighbouring amino group in Ser-216 forming a sulfenamide.[47] On this basis, one may speculate that the formation of the cyclic sulfenamide in levesquamide occurs through a similar mechanism in which the thiol group in a levesquamide intermediate can be oxidized by ROS and form a sulfenic acid intermediate. Alternatively, the four oxidase candidates from BGC1 described above may be involved in thiol oxidation. Following oxidation, LvqR may be involved in reduction of the oxidized sulfur atom to reverse any overoxidation. LvqP encodes a thioredoxin likely participating in restoration of LvqR catalytic activity. Additionally, LvqS

encodes a pyridine nucleotide-disulfide oxidoreductase, which was reported to catalyze the disulfide bond formation in FK228,[37] indicating the formation of the sulfenamide moiety in **1** may proceed through a disulfide intermediate (Scheme 2).

Scheme 2. Proposed NRPS post-modification steps after levesquamide (1) has been released from the thioreductase.

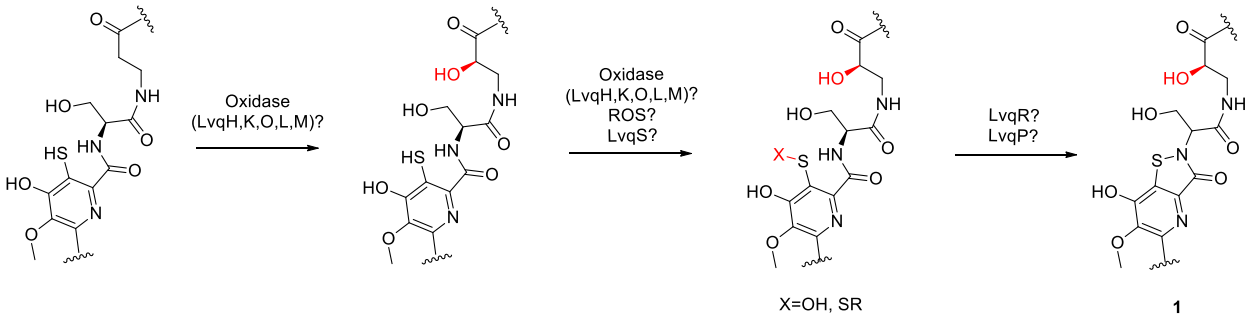

Bioactivities. Due to its structural novelty, levesquamide (**1**) was assessed for a variety of biological activities. Antimicrobial testing uncovered potent antitubercular activity against *M. tuberculosis* H37Ra ATCC 25177, exhibiting an IC_{50} value of 1.33 μM. The antimicrobial activity of **1** against the virulent *M. tuberculosis* strain H37Rv ATCC 27294 was then assessed. The minimum inhibitory concentrations (MICs) in the microplate alamarBlue assay (MABA) and low oxygen recovery assay (LORA)[48] were 9.65 and 22.28 μM, respectively. The MABA is used to assess growth inhibition of actively growing *M. tuberculosis* under aerobic conditions, while the LORA is used to assess inhibition against non-replicating persisters under hypoxic conditions.[48] Although eradicating non-replicating *M. tuberculosis* is essential to successfully treat tuberculosis infections, most current drugs are ineffective against non-replicating persisters and require long treatment durations.[49] The effectiveness of **1** against rifampicin- (RIF^R) and isoniazid-resistant (INH^R) *M. tuberculosis* strains was assessed using the MABA assay. The antimicrobial activity of **1** against the resistant strains was essentially identical to that observed against the parental strain (MICs, RIF^R 9.46 μM, INH^R 9.90 μM). In comparison, rifampicin and isoniazid were 100- and 20-fold less active against the corresponding resistant strain (Table 3). This data suggests **1** has a different mode of action than rifampicin and isoniazid. Despite having a lower potency than PA824 and TMC207, two second-line drugs used to treat multi-drug resistant tuberculosis infections, **1** may prove to be a promising drug lead as structural optimization may improve its potency. A synthetic sulfur-containing heterocyclic compound BTZ043 was proven to be a potent inhibitor of decaprenylphosphoryl-β-D-ribose 2′-epimerase in drug-sensitive and drug-resistant *M. tuberculosis* strains.[50] The sulfur-containing heterocycle in BTZ043 may be critical for the activity, thus further testing levesquamide against this target enzyme will be a reasonable first-step in understanding its mode of action.

The antimicrobial activity of **1** appears to be relatively selective for *M. tuberculosis*, as it showed relatively weak activity against methicillin-resistant *Staphylococcus aureus* ATCC 33591 (IC_{50} value of 104.32 μM) and was inactive against vancomycin-resistant *Enterococcus faecium*

EF379, *S. warneri* ATCC 17917, *Pseudomonas aeruginosa* ATCC 14210, *Proteus vulgaris* ATCC 12454, and *Candida albicans* ATCC 14035 at the highest concentration tested (203 μM).

To assess cytotoxicity against human cells, the activity of **1** was tested against the normal CCL-81 Vero kidney cell line and the MCF7 (breast), HTB26 (breast) and HCT116 (colon) cancer cell lines. No growth inhibition was observed at the maximum tested concentration (51 μM), indicating **1** is not cytotoxic against mammalian cell lines.

Table 3. MICs (μM) of **1** in MABA and LORA assays against *M. tuberculosis* H37Rv ATCC 27294.

Compound	H37Rv		Rifampicin-resistant strain	Isoniazid-resistant strain
	MABA	LORA	MABA	MABA
1	9.65	22.28	9.46	9.90
Rifampicin	0.01	0.05	>1.22	<0.005
Isoniazid	2.70	305.03	10.65	>58.35
PA824	0.42	14.14	2.92	2.23
TMC207	0.04	0.18	0.04	0.05

CONCLUSION

Elucidating the structure of levesquamide (**1**) by NMR spectroscopy was a significant challenge due to the presence of the proton-deficient fused pyridine-isothiazolinone moiety. Characterization of the BGC of **1** allowed us to predict the structure of this uncommon moiety based on similarity to the collismycin BGC. This finding guided a series of stable isotope labeling experiments, which ultimately enabled us to solve the structure of **1**. Identification of the levesquamide BGC provided an opportunity to shed light on isothiazolinone biosynthesis, although further studies on the levesquamide BGC will be required to determine the precise mechanism of sulfur-nitrogen bond formation. Oxidized levesquamide analogs were observed from LC-HRMS analysis, suggesting putative pathways of thiol oxidation that may lead to the formation of the cyclic sulfenamide. Levesquamide (**1**) also exhibited promising antitubercular activity against antibiotic-resistant strains of the important human pathogen *M. tuberculosis*. The pharmacological properties of **1** are currently under investigation to further explore its potential as a future tuberculosis treatment. Identification of the levesquamide BGC has also set the stage for future genetic engineering studies to modify the structure and improve the properties of **1** to drive future clinical development of this promising new marine natural product.

EXPERIMENTAL PROCEDURES

General Methods. All commercially available solvents and reagents were used without further purification. Deionized water was purified to 18.2 MΩ·cm on a Milli-Q® Biocel water

purification system (EMD Millipore). Automated reversed-phase medium pressure liquid chromatography (RP-MPLC) was performed on a Combi*Flash* Rf (Teledyne Isco) equipped with a photodiode array (PDA) detector. Reversed-phase high-performance liquid chromatography (RP-HPLC) was performed on an Accela^{TM} chromatography system (Thermo Fisher Scientific) equipped with a PDA and evaporative light scattering detector (ELSD; Sedex 80). All ^{1}H, ^{13}C, and ^{15}N NMR spectra were acquired on a 600 MHz or a 400 MHz Bruker Avance III NMR spectrometer. All carbon and proton chemical shifts were reported in δ units (ppm) and were referenced to the residual solvent signals (CD_3OD: δ_H 7.26 ppm and δ_C 77.16 ppm; DMSO-*d*$_6$: δ_H 2.50 ppm and δ_C 39.52 ppm), while nitrogen chemical shifts were calibrated via indirect referencing[14]. Coupling constants were reported in Hz with the following abbreviations: (s) singlet, (d) doublet, (t) triplet, (m) multiplet, (app.) apparent pattern.

UHPLC-HRMS and tandem mass spectra were recorded on a Thermo LTQ Orbitrap Velos mass spectrometer operating with an ESI positive mode. The system was controlled by XCalibur 2.2 software (ThermoScientific). UHPLC-HRMS analysis was using a Core-Shell 100Å C18 column (Phenomenex, Kinetex, 1.7µm 50 × 2.1mm), operating on a resolution of 30,000, monitoring a mass range from 190 to 2000 atomic mass units (amu). A linear solvent gradient from 95% H_2O / 0.1% formic acid (solvent A) and 5% CH_3CN / 0.1% formic acid (solvent B) to 100% solvent B over 4.8 min followed by a hold for 3.2 min with a flow rate of 500 µL/min and 10 µL injection volume was used. Eluent was detected by ESI-HRMS, ELSD and UV 200−600 nm. UV spectra were acquired by injection of a pure sample in the UHPLC-HRMS system with background subtraction in Xcalibur.

Tandem mass spectrometry analysis was performed using direct infusion with a resolution of 30,000, monitoring a mass range from 50-2000 amu. Selected ions were fragmented under CID. The mass spectrometer was operated under the following conditions: spray voltage, 3.0 kV; capillary temperature, 300°C; S-lens RF voltage, 60.0%; maximum injection time (ms), 10; microscans, 1.

Marfey's analysis was performed using an UHPLC-HRMS experiment using the aforementioned system with a flow rate of 400 µL/min and a linear gradient over 55 min from H_2O : CH_3CN : formic acid (95% : 5% : 0.1%) to H_2O: CH_3CN : formic acid (60% : 40%: 0.1%) then another linear gradient over 2 min to 100% CH_3CN with formic acid (0.1%) followed by 3 min at 100% CH_3CN with formic acid (0.1%), and an additional 10 min of re-equilibration period with the initial conditions.

Infrared spectra were acquired by attenuated total reflectance using a SMART iTR^{TM} accessory on a Nicolet^{TM} 6700 FTIR spectrometer (Thermo Fisher Scientific). PCR reactions were performed using Mastercycler$^{®}$ nexus (Eppendorf).

Isolation, Fermentation, and Extraction. *Streptomyces* sp. RKND-216 was isolated from marine sediment collected from Burnt Point, PE, Canada (46.170339, -62.505634) at a depth of 13 m. A two-stage seed culture process was used to generate inocula. The strain was maintained on marine ISP2[51] (ISP2m; ISP2 supplemented with 18 g/L instant ocean) agar plates incubated at 30°C. Approximately 1 cm^2 of the agar culture was used to inoculate 7 mL of ISP2m broth in a

25 x 150 mm culture tube containing 5 4-mm glass beads and incubated at 30°C and 200 rpm. After 72 h, 1 mL of the first-stage seed was transferred to 7 mL of fresh ISP2m broth and incubated under the same conditions for 24 h. The second-stage seeds from multiple tubes were combined, and 30 mL of seed culture was used to inoculate each of 6 Fernbach flasks containing 1 L of fresh ISP2m broth each. After incubating for 6 days at 30°C with shaking at 200 rpm, the culture was extracted three times with equal volumes of EtOAc. The organic layers were combined and dried *in vacuo*.

Chromatographic Purification. The *Streptomyces* sp. RKND-216 crude extract (0.9 g) was prepared for solid load injection by adsorbing on C_{18} and the separation was performed with a 130 g C_{18} column (RediSep Rf®) using a mobile phase flow rate of 32 mL/min. The mobile phase consisted of a linear gradient from CH_3OH : H_2O (5% : 95%) to 100% CH_3OH over 21 min followed by 100% CH_3OH for 5 min. Levesquamide was further purified by reversed-phase high-performance liquid chromatography (RP-HPLC) using a semi-preparative Luna C_{18} 100 Å column (250 × 10 mm, 5 μm; Phenomenex, 213436-1). An isocratic elution with 35 % H_2O containing 0.1% formic acid and 65% CH_3OH containing 0.1% formic acid was used. The eluent was monitored by ELSD, and UV at 277 and 348 nm while **1** was collected at 23.2 min. Subsequent evaporation *in vacuo* resulted in 2 mg of pure compound **1**.

*Levesquamide (**1**):* white solid; UV λ_{max} 277, 348 nm; IR ν_{max} 3484, 3371, 3341, 3282, 2948, 2908, 1652, 1634, 1622, 1598, 1544, 1521, 1494 cm^{-1}; ^1H NMR (DMSO-d_6, 600 MHz) and ^{13}C NMR (DMSO-d_6, 150 MHz) data are described in Table 1; HRESIMS *m/z* $[M+H]^+$ 631.2180 (calcd for $C_{28}H_{35}O_9N_6S$, 631.2181).

Stable Isotope Labeling Fermentations. Sodium [1,2-$^{13}C_2$] acetate (0.5 g/L), 0.036 g/L L-[1,2,3-$^{13}C_3$, ^{15}N] cysteine, and 0.6 g/L [^{15}N] ammonium chloride were individually supplemented at the time of inoculation to 1 L of a modified lean medium[52] consisting of glucose 0.04 %, galactose 0.08 %, maltose 0.08 %, dextrin 0.16 %, Bacto-Soytone (Difco) 0.08 %, NH_4Cl 0.06 %, and Instant Ocean 1.8 %, while a double labeling experiment was performed when both 0.5 g/L sodium [1,2-$^{13}C_2$] acetate, 0.036 g/L L-[1,2,3-$^{13}C_3$, ^{15}N] cysteine were added to 1.7 L of the fermentation medium at the time of inoculation. Seed cultivation, fermentation and purification conditions were the same as described above.

Genome Sequencing, Assembly and Annotation. Genomic DNA was isolated from *Streptomyces* sp. RKND-216 cells obtained from 1.8 mL of culture in marine ISP2 using the DNeasy® UltraClean® Microbial Kit (Qiagen). Genome sequencing was performed using the Pacific Biosciences RS II platform and assembled using Hierarchical Genome Assembly Process (HGAP) by the Genome Quebec Innovation Centre.[18] AntiSMASH 5.0.0[12] and PRISM4[17] were used to annotate secondary metabolite biosynthetic gene clusters in the genome. Protein alignments used to analyze the substrate specificity codes of NRPS A and CAL domains were prepared using Clustal Omega[53]. Consensus A domain specific codes were extracted from previously reported A domain sequences,[54] and sequence logo plots were prepared using WebLogo[55].

Construction of knockout plasmid pLLKO_lvqF. To construct an in-frame deletion in *lvqF*, a double cross over gene replacement strategy was used. Plasmid pLLKO_lvqF was constructed by assembling two fragments (lvqF_A and lvqF_B) flanking a 339 bp deletion (lvqFdel) spanning the S-adenosylmethionine binding site of LvqF using a Gibson assembly strategy. Primers for Gibson assembly were designed using the NEB Builder Assembly Tool (v 2.2.5; http://nebuilder.neb.com). The flanking DNA fragments were generated by PCR (Phusion® Hot Start Flex DNA Polymerase; New England Biolabs) from genomic DNA of *Streptomyces* sp. RKND-216. Upstream fragment (lvqF_A, 1,006 bp) consisting of 922 bp upstream of the *lvqF* start codon and the first 84 bp nucleotides of *lvqF* was amplified using the primers Orf255KO_A_F and Orf255KO_A_R (Table S4). The downstream fragment (lvqF_B, 883 bp) fragment (consisting of the last 198 bp of *lvqF* and 685 bp of downstream of the *lvqF* stop codon were amplified using the primers Orf255KO_B_F and Orf255KO_B_R (Table S4). pKC1139[56] was digested with XbaI and EcoRI. pKC1139, lvqF_A and lvqF_B were assembled using the Gibson Assembly Master Mix (New England Biolabs) according to the manufacturer's recommendations. Gibson Assembly reactions were used to transformed 5-alpha chemically competent *E. coli* (New England Biolabs). Plasmid DNA was purified from apramycin-resistant transformants using the QIAprep Spin Miniprep Kit (Qiagen). The sequences of correctly assembled plasmids were confirmed by dideoxy terminator sequencing the assembled insert in pKC1139 performed by Eurofins Genomics (Toronto, ON) using primers M13_F, 600_F, 1246_F, 1608_F, M13_R, 671_R, 1208_R, 2003_R (Table S4).

Construction of complementation plasmids. To compliment *lvqF* deletion mutants a complementation plasmid carrying *lvqF* under control of the constitutive *ermE** promoter was constructed (pLLermE*_lvqF) using Gibson Assembly. Primers to amplify the *ermE*p* and *lvqF* were designed as described above. PCR was performed using Phusion® Hot Start Flex DNA Polymerase (New England Biolabs). A 287 bp fragment containing the *ermE*p* was amplified from pSE34[57] using the primers ErmE*_F and ErmE*_R and a 645 bp fragment (lvqF_RBS) consisting of *lvqF* and its ribosomal binding site was amplified using the primers LvqF_RBS_F and LvqF_RBS_R (Table S4). pKC1139 was digested with XbaI/EcoRI and assembled with the *ermE*p* and *lvqF* fragments using the Gibson Assembly Master Mix (New England Biolabs) according to the manufacturer's recommendations. Transformation of Gibson Assembly reactions and plasmid isolation were performed as described above. The sequences of correctly assembled plasmids were confirmed by dideoxy terminator sequencing the assembled insert in pKC1139 performed by Eurofins Genomics (Toronto, ON) using primers M13_F, M13_R, and 242_258_F (Table S4). To prepare a control expression plasmid (pLLermE*), pLLermE*_lvqF was digested with EcoRI and BamHI to excise *lvqF*. The linearized plasmid was treated with mung bean nuclease (New England Biolabs) to create blunt ends. The 6.8 kb fragment containing pKC1139 and the *ermE*p* was purified following agarose gel electrophoresis using the QIAquick Gel Extraction Kit (Qiagen) and the DNA fragment was circularized with T4 DNA ligase (Invitrogen) according the manufacture's recommendation. Transformation and DNA isolation was performed as described above. The sequences of correctly assembled plasmids were confirmed by dideoxy terminator sequencing the assembled insert in pKC1139 performed by Eurofins Genomics (Toronto, ON) using primers M13_F and M13_R (Table S4).

***lvqF* inactivation and Complementation.** Inactivation of *lvqF* was achieved using a double crossover gene replacement strategy. *Streptomyces* sp. RKND-216 spores were harvested from confluent cultures cultured on ISP4[51] agar plates. Spores were collected by centrifugation (5,000*g*, 10 min) and washed with 1 mL of 2XYT (1.6% tryptone, 1% yeast extract, 0.5% sodium chloride) and then suspended in 2XYT at a cell density of approximately10^9 cfu/mL. To facilitate intergeneric conjugation between *E. coli* and *Streptomyces* plasmids were used to transform *E. coli* ET12567::pUZ8002 and transformants were selected on LB agar supplemented with apramycin, kanamycin and chloramphenicol (25 µg/mL each). For conjugation, *E. coli* strains were cultured in LB broth (50 mL) containing 25 µg/mL apramycin at 37 °C and 250 rpm to an OD_{600} of approximately 0.4. The cells were pelleted and washed with 2XYT medium twice before suspending in 3 mL of 2XYT. Equal volumes (0.5 mL) of *E. coli* and RKND-216 spores were combined and then the cells collected by centrifugation 5,000*g,*10 min) and then suspended in 300 µL 2XYT. Aliquots (100 µL) of the cell mixture were spread on ISP4m agar plates containing 10 mM $CaCl_2$ and incubated at 37 °C for 18 h. The plates were then overlaid with 1 mL of sterile H_2O containing 50 µg of nalidixic acid and 25 µg apramycin and further incubated at 30 °C for 7 days. To select for *lvqF* deletion mutants, exconjugants were cultured on ISP2m plates without apramycin selection for multiple rounds of growth. Potential deletion mutants (apramycin sensitive) were identified by plating exconjugants on marine ISP4 agar containing 25 µg/mL apramycin. Deletion mutants were identified by colony PCR. Cells of patched mutants were suspended in DMSO to lyse cells and the lysed cells were used as template in PCR reactions using the primers 50502F and 51807R (Table S4). The primers were manually designed to amplify a 1305 bp fragment from the wild-type and a 966 bp fragment from mutants.

For complementation experiments spores of *Streptomyces* sp. RKND-216 Δ*lvqF* were harvested from ISP4m plates. Conjugation between RKND-216 Δ*lvqF* and *E. coli* ET12567::pUZ8002::pLLermE*_lvqF or *E. coli* ET12567::pUZ8002::pLLermE* was performed following the aforementioned methods. Exconjugants were selected on LB agar supplemented with 25 µg/mL apramycin.

Analysis of Wild-Type and Mutant Strains. *Streptomyces* sp. RKND-216 ΔlvqF, *Streptomyces* sp. RKND-216 ΔlvqF::pLLermE*_lvqF and *Streptomyces* sp. RKND-216 ΔlvqF::pLLermE* were fermented in 7 mL of ISP2m medium at 30 °C and 200 rpm for 6 days. Fermentations were extracted three times with 7 mL of EtOAc. The EtOAc layers were combined and re-suspended in 1 mL of MeOH for UHPLC-HRMS analysis.

Antimicrobial Assays and Cytotoxicity Assays. Anti-mycobacterial activities against *Mycobacterium tuberculosis* strain H37Ra (ATCC 25177) were performed at the University of New Brunswick as described previously[58]. Microplate alamarBlue assay (MABA) and low oxygen recovery assay (LORA) against *M. tuberculosis* H37Rv (ATCC 27294) and drug-resistant strains were evaluated at the Institute for Tuberculosis Research at University of Illinois Chicago using literature protocols[45]. Anti-microbial activities against methicillin-resistant *Staphylococcus aureus* ATCC 33591, vancomycin-resistant *Enterococci faecium* EF379, *S. warneri* ATCC 17917, *Pseudomonas aeruginosa* ATCC 14210, *Proteus vulgaris* ATCC 12454, and *Candida albicans* ATCC 14035, as well as cytotoxicity assays against CCL-81 Vero kidney

cells, MCF7 breast cancer cells, HTB26 breast cancer cells and HCT116 colon cancer cells were evaluated using the protocol described by Overy and co-workers[59].

Supporting Information

The Supporting Information is available free of charge on the ACS Publication website at DOI: xxx

Supplementary figures and tables, and all spectroscopic data.

Corresponding Author

*rkerr@upei.ca

Author Contributions

L.L., B.H., D.M., and R.K. conceptualized the project. L.L. and D.M. performed the chemical isolation and characterization, M.F. and C.K. facilitated NMR data acquisition, H.C. helped with LC-MS instrumentation. L.L. and B.H. performed the bioinformatics and molecular biology experiments. T.C. and C.G. performed the initial bioassays against *M. tuberculosis* H37Ra ATCC 25177. L.L., B.H., D.M., and R.K. wrote the manuscript.

Notes

The authors declare no competing financial interests.

Acknowledgements

The authors gratefully acknowledge Baojie Wan and Scott G. Franzblau at Institute for Tuberculosis Research, University of Illinois at Chicago for conducting MABA and LORA assays against *M. tuberculosis* strains. The work was supported by Innovation PEI, Natural Sciences and Engineering Council of Canada, the Canada Research Chair Program, the Atlantic Canada Opportunities Agency, Canada Foundation for Innovation, Nautilus Biosciences Croda, and the Jeanne and Jean-Louis Lévesque Foundation.

References

(1) Petkowski, J. J.; Bains, W.; Seager, S. Natural products containing a Nitrogen–Sulfur bond. *J. Nat. Prod.* **2018***, 81*, 423-446.

(2) Devys, M.; Barbier, M.; Loiselet, I.; Rouxel, T.; Sarniguet, A.; Kollmann, A.; Bousquet, J. Brassilexin, a novel sulphur-containing phytoalexin from Brassica juncea L., (cruciferae). *Tetrahedron Lett.* **1988***, 29*, 6447-6448.

(3) Soledade, M.; Pedras, C.; Smith, K. C. Sinalexin, a phytoalexin from white mustard elicited by destruxin B and *Alternaria brassicae*. *Phytochemistry* **1997***, 46*, 833-837.

(4) Stratmann, K.; Belli, J.; Jensen, C. M.; Moore, R. E.; Patterson, G. M. Aulosirazole, a novel solid tumor selective cytotoxin from the blue-green alga *Aulosira fertilissima*. *J. Org. Chem.* **1994***, 59*, 6279-6281.

(5) Nakae, K.; Adachi, H.; Sawa, R.; Hosokawa, N.; Hatano, M.; Igarashi, M.; Nishimura, Y.; Akamatsu, Y.; Nomoto, A. NAD (P) H quinone oxidoreductase 1 (NQO1)-bioactivated pronqodine A regulates prostaglandin release from human synovial sarcoma cells. *J. Nat. Prod.* **2013***, 76*, 510-515.

(6) (a) Gomi, S.; Amano, S.; Sato, E.; Miyadoh, S.; Kodama, Y. Novel antibiotics SF2738A, B and C, and their analogs produced by *Streptomyces* sp. *J. Antibiot.* **1994***, 47*, 1385-1394. (b) Garcia, I.; Vior, N. M.; Braña, A. F.; González-Sabin, J.; Rohr, J.; Moris, F.; Méndez, C.; Salas, J. A. Elucidating the biosynthetic pathway for the polyketide-nonribosomal peptide collismycin A: mechanism for formation of the 2, 2′-bipyridyl ring. *Chem. Biol.* **2012***, 19*, 399-413. (c) Chen, D.; Zhao, Q.; Liu, W. Discovery of caerulomycin/collismycin-type 2, 2′-bipyridine natural products in the genomic era. *J. Ind. Microbiol. Biot.* **2019**, *46*, 459-468.

(7) Stadler, M.; Bauch, F.; Henkel, T.; Mühlbauer, A.; Müller, H.; Spaltmann, F.; Weber, K. Antifungal actinomycete metabolites discovered in a differential cell-based screening using a recombinant TOPO1 deletion mutant strain. *Archiv der Pharmazie: An International Journal Pharmaceutical and Medicinal Chemistry* **2001***, 334*, 143-147.

(8) Shindo, K.; Yamagishi, Y.; OKada, Y.; Kawai, H. Collismycins A and B, novel non-steroidal inhibitors of dexamethasone-glucocorticoid receptor binding. *J. Antibiot.* **1994***, 47*, 1072-1074.

(9) Gil, A. M.; Egea, P. U.; Padilla, M. M.; Palomero, E. G.; Baz, J. P.; Chimeno, R. I. F.; Fernandez, A. M.; Hernandez, L. M. C.; Millan, F. R.; Morera, A. C. Use of collismycin and derivatives thereof as oxidative stress inhibitors. U.S. Patent WO 8067441, November 29, 2011.(10) (a) McInnes, A. G.; Smith, D. G.; Walter, J. A.; Vining, L. C.; Wright, J. L. The biosynthesis of caerulomycin A in *Streptomyces caeruleus*. Incorporation of 14C-and 13C-labeled precursors and analyses of labeling patterns by 13C nmr. *Canadian Journal of Chemistry* **1979***, 57*, 3200-3204. (b) Vining, L. C.; McInnes, A. G.; McCulloch, A. W.; Smith, D. G.; Walter, J. A. The biosynthesis of caerulomycins in *Streptomyces caeruleus*. Isolation of a new caerulomycin and incorporation of picolinic acid and glycerol into caerulomycin A. *Canadian journal of chemistry* **1988***, 66*, 191-194.

(11) Qu, X.; Pang, B.; Zhang, Z.; Chen, M.; Wu, Z.; Zhao, Q.; Zhang, Q.; Wang, Y.; Liu, Y.; Liu, W. Caerulomycins and collismycins share a common paradigm for 2, 2′-bipyridine biosynthesis via an unusual hybrid polyketide–peptide assembly logic. *J. Am. Chem. Soc.* **2012***, 134*, 9038-9041.

(12) Blin, K.; Shaw, S.; Steinke, K.; Villebro, R.; Ziemert, N.; Lee, S. Y.; Medema, M. H.; Weber, T. antiSMASH 5.0: updates to the secondary metabolite genome mining pipeline. *Nucleic Acids Res.* **2019**, *47*, W81-W87.

(13) Kalyon, B.; Helaly, S. E.; Scholz, R.; Nachtigall, J.; Vater, J.; Borriss, R.; Süssmuth, R. D. Plantazolicin A and B: structure elucidation of ribosomally synthesized thiazole/oxazole peptides from *Bacillus amyloliquefaciens* FZB42. *Org. Lett.* **2011***, 13*, 2996-2999.

(14) Harris, R. K.; Becker, E. D.; De Menezes, Sonia M Cabral; Goodfellow, R.; Granger, P. NMR nomenclature. Nuclear spin properties and conventions for chemical shifts (IUPAC Recommendations 2001). *Pure and Applied Chemistry* **2001***, 73*, 1795-1818.

(15) Tatusova, T.; DiCuccio, M.; Badretdin, A.; Chetvernin, V.; Nawrocki, E. P.; Zaslavsky, L.; Lomsadze, A.; Pruitt, K. D.; Borodovsky, M.; Ostell, J. NCBI prokaryotic genome annotation pipeline. *Nucleic Acids Res.* **2016***, 44*, 6614-6624.

(16) (a) Weber, T.; Blin, K.; Duddela, S.; Krug, D.; Kim, H. U.; Bruccoleri, R.; Lee, S. Y.; Fischbach, M. A.; Muller, R.; Wohlleben, W.; Breitling, R.; Takano, E.; Medema, M. H. antiSMASH 3.0-a comprehensive resource for the genome mining of biosynthetic gene clusters. *Nucleic Acids Res.* **2015***, 43*, W237-43. (b) Blin, K.; Wolf, T.; Chevrette, M. G.; Lu, X.; Schwalen, C. J.; Kautsar, S. A.; Suarez Duran, H. G.; de Los Santos, Emmanuel LC; Kim, H. U.; Nave, M. antiSMASH 4.0—improvements in chemistry prediction and gene cluster boundary identification. *Nucleic Acids Res.* **2017***, 45*, W36-W41.

(17) Skinnider, M. A.; Dejong, C. A.; Rees, P. N.; Johnston, C. W.; Li, H.; Webster, A. L.; Wyatt, M. A.; Magarvey, N. A. Genomes to natural products prediction informatics for secondary metabolomes (PRISM). *Nucleic Acids Res.* **2015***, 43*, 9645-9662.

(18) Liang, L.; Haltli, B. A.; Kerr, R. G. Draft genome sequence of *Streptomyces* sp. strain RKND-216, an antibiotic producer isolated from marine sediment in Prince Edward Island, Canada. *Microbiology Resource Announcements* **2019***, 8*, e00870-19.

(19) Du, L.; Sánchez, C.; Chen, M.; Edwards, D. J.; Shen, B. The biosynthetic gene cluster for the antitumor drug bleomycin from *Streptomyces verticillus* ATCC15003 supporting functional interactions between nonribosomal peptide synthetases and a polyketide synthase. *Chem. Biol.* **2000***, 7*, 623-642.

(20) Stachelhaus, T.; Mootz, H. D.; Marahiel, M. A. The specificity-conferring code of adenylation domains in nonribosomal peptide synthetases. *Chem. Biol.* **1999***, 6*, 493-505.

(21) Coleman, J. P.; Hudson, L. L.; McKnight, S. L.; Farrow, J. M.,3rd; Calfee, M. W.; Lindsey, C. A.; Pesci, E. C. *Pseudomonas aeruginosa* PqsA is an anthranilate-coenzyme A ligase. *J. Bacteriol.* **2008***, 190*, 1247-1255.

(22) Ames, B. D.; Walsh, C. T. Anthranilate-activating modules from fungal nonribosomal peptide assembly lines. *Biochemistry (N. Y.)* **2010***, 49*, 3351-3365.

(23) Schneider, T. L.; Shen, B.; Walsh, C. T. Oxidase domains in epothilone and bleomycin biosynthesis: thiazoline to thiazole oxidation during chain elongation. *Biochemistry (N. Y.)* **2003***, 42*, 9722-9730.

(24) Marchler-Bauer, A.; Bo, Y.; Han, L.; He, J.; Lanczycki, C. J.; Lu, S.; Chitsaz, F.; Derbyshire, M. K.; Geer, R. C.; Gonzales, N. R. CDD/SPARCLE: functional classification of proteins via subfamily domain architectures. *Nucleic Acids Res.* **2016***, 45*, D200-D203.

(25) Schümperli, D.; McKenney, K.; Sobieski, D. A.; Rosenberg, M. Translational coupling at an intercistronic boundary of the *Escherichia coli* galactose operon. *Cell* **1982***, 30*, 865-871.

(26) (a) Konz, D.; Marahiel, M. A. How do peptide synthetases generate structural diversity? *Chem. Biol.* **1999***, 6*, R39-R48. (b) Stachelhaus, T.; Walsh, C. T. Mutational analysis of the epimerization domain in the initiation module PheATE of gramicidin S synthetase. *Biochemistry (N. Y.)* **2000***, 39*, 5775-5787.

(27) Röttig, M.; Medema, M. H.; Blin, K.; Weber, T.; Rausch, C.; Kohlbacher, O. NRPSpredictor2—a web server for predicting NRPS adenylation domain specificity. *Nucleic Acids Res.* **2011***, 39*, W362-W367.

(28) Wojciechowska, H.; Zgoda, W.; Borowski, E.; Dziegielewski, K.; Ulikowski, S. The antibiotc edeine. XII. *J. Antibiot.* **1983***, 36*, 793-798.

(29) Schmidt, E. W.; Bewley, C. A.; Faulkner, D. J. Theopalauamide, a bicyclic glycopeptide from filamentous bacterial symbionts of the lithistid sponge *Theonella swinhoei* from Palau and Mozambique. *J. Org. Chem.* **1998**, *63*, 1254-1258.

(30) Mori, T.; Cahn, J. K.; Wilson, M. C.; Meoded, R. A.; Wiebach, V.; Martinez, A. F. C.; Helfrich, E. J.; Albersmeier, A.; Wibberg, D.; Dätwyler, S.; Keren, R.; Lavy, A.; Ruckert C.; Ilan M., Kalinowski J.; Matsunaga S.; Takeyama H.; Piel J. Single-bacterial genomics validates rich and varied specialized metabolism of uncultivated *Entotheonella* sponge symbionts. *Proc. Natl. Acad. Sci. U. S. A.* **2018**, *115*, 1718-1723.

(31) Iftime, D.; Kulik, A.; Härtner, T.; Rohrer, S., Niedermeyer, T. H. J.; Stegmann, E.; Weber, T., Wohlleben, W. Identification and activation of novel biosynthetic gene clusters by genome mining in the kirromycin producer *Streptomyces collinus* Tü 365. *J. Ind. Microbiol. Biotechnol.* **2016**, *43*, 277-291.

(32) Du, L.; Lou, L. PKS and NRPS release mechanisms. *Nat. Prod. Rep.* **2010***, 27*, 255-278.

(33) Schwarzer, D.; Mootz, H. D.; Linne, U.; Marahiel, M. A. Regeneration of misprimed nonribosomal peptide synthetases by type II thioesterases. *Proc. Natl. Acad. Sci. U. S. A.* **2002***, 99*, 14083-14088.

(34) He, P.; Moran, G. R. Structural and mechanistic comparisons of the metal-binding members of the vicinal oxygen chelate (VOC) superfamily. *J. Inorg. Biochem.* **2011***, 105*, 1259-1272.

(35) (a) Poole, L. B. Bacterial defenses against oxidants: mechanistic features of cysteine-based peroxidases and their flavoprotein reductases. *Arch. Biochem. Biophys.* **2005***, 433*, 240-254. (b) Rocha, E. R.; Smith, C. J. Role of the alkyl hydroperoxide reductase (ahpCF) gene in oxidative stress defense of the obligate anaerobe *Bacteroides fragilis*. *J. Bacteriol.* **1999***, 181*, 5701-5710.

(36) Holmgren, A. Thioredoxin structure and mechanism: conformational changes on oxidation of the active-site sulfhydryls to a disulfide. *Structure* **1995***, 3*, 239-243.

(37) Wang, C.; Wesener, S. R.; Zhang, H.; Cheng, Y. An FAD-dependent pyridine nucleotide-disulfide oxidoreductase is involved in disulfide bond formation in FK228 anticancer depsipeptide. *Chem. Biol.* **2009***, 16*, 585-593.

(38) Chen, F.; Lin, L.; Wang, L.; Tan, Y.; Zhou, H.; Wang, Y.; Wang, Y.; He, W. Distribution of dTDP-glucose-4, 6-dehydratase gene and diversity of potential glycosylated natural products in marine sediment-derived bacteria. *Appl. Microbiol. Biotechnol.* **2011***, 90*, 1347-1359.

(39) Davidson, A. L.; Alvarez, F. J. Binding protein-dependent uptake of maltose intocells via an ATP-binding cassette transporter. *EcoSal Plus* **2010***, 4*, 10.1128/ecosalplus.3.3.3.

(40) Kumar, S.; He, G.; Kakarla, P.; Shrestha, U.; KC, R.; Ranaweera, I.; Mark Willmon, T.; R Barr, S.; J Hernandez, A.; F Varela, M. Bacterial multidrug efflux pumps of the major facilitator superfamily as targets for modulation. *Infectious Disorders-Drug Targets (Formerly Current Drug Targets-Infectious Disorders)* **2016***, 16*, 28-43.

(41) Bibb, M. J.; Janssen, G. R.; Ward, J. M. Cloning and analysis of the promoter region of the erythromycin resistance gene (ermE) of *Streptomyces erythraeus*. *Gene* **1985***, 38*, 215-226.

(42) Li, Y.; Liu, J.; Adekunle, D.; Bown, L.; Tahlan, K.; Bignell, D. R. TxtH is a key component of the thaxtomin biosynthetic machinery in the potato common scab pathogen *Streptomyces scabies*. *Molecular plant pathology* **2019***, 20*, 1379-1393.

(43) Piotto, M., Bourdonneau, M., Elbayed, K., Wieruszeski, J. M., Lippens, G. New DEFT sequences for the acquisition of one-dimensional carbon NMR spectra of small unlabelled molecules. *Magn. Reson. Chem.* **2006**, *44*, 943-947.

(44) Garcia, I.; Vior, N. M.; González-Sabín, J.; Braña, A. F.; Rohr, J.; Moris, F.; Méndez, C.; Salas, J. A. Engineering the biosynthesis of the polyketide-nonribosomal peptide collismycin A for generation of analogs with neuroprotective activity. *Chem. Biol.* **2013***, 20*, 1022-1032.

(45) (a) Zhu, Y.; Zhang, Q.; Li, S.; Lin, Q.; Fu, P.; Zhang, G.; Zhang, H.; Shi, R.; Zhu, W.; Zhang, C. Insights into caerulomycin A biosynthesis: A two-component monooxygenase CrmH-catalyzed oxime formation. *J. Am. Chem. Soc.* **2013***, 135*, 18750-18753. (b) Zhu, Y.; Xu, J.; Mei, X.; Feng, Z.; Zhang, L.; Zhang, Q.; Zhang, G.; Zhu, W.; Liu, J.; Zhang, C. Biochemical and structural insights into the aminotransferase CrmG in caerulomycin biosynthesis. *ACS chemical biology* **2016***, 11*, 943-952.

(46) (a) Dubbs, J. M.; Mongkolsuk, S. Peroxide-sensing transcriptional regulators in bacteria. *J. Bacteriol.* **2012***, 194*, 5495-5503. (b) Defelipe, L. A.; Lanzarotti, E.; Gauto, D.; Marti, M. A.; Turjanski, A. G. Protein topology determines cysteine oxidation fate: the case of sulfenyl amide formation among protein families. *PLoS computational biology* **2015***, 11*, e1004051. (c) Poole, L. B. The basics of thiols and cysteines in redox biology and chemistry. *Free Radical Biology and Medicine* **2015***, 80*, 148-157.

(47) (a) Sivaramakrishnan, S.; Cummings, A. H.; Gates, K. S. Protection of a single-cysteine redox switch from oxidative destruction: on the functional role of sulfenyl amide formation in the redox-regulated enzyme PTP1B. *Bioorg. Med. Chem. Lett.* **2010***, 20*, 444-447. (b) van Montfort, R. L.; Congreve, M.; Tisi, D.; Carr, R.; Jhoti, H. Oxidation state of the active-site cysteine in protein tyrosine phosphatase 1B. *Nature* **2003***, 423*, 773. (c) Salmeen, A.; Andersen, J. N.; Myers, M. P.; Meng, T.; Hinks, J. A.; Tonks, N. K.; Barford, D. Redox regulation of protein tyrosine phosphatase 1B involves a sulphenyl-amide intermediate. *Nature* **2003***, 423*, 769. (d) Lee, J. W.; Soonsanga, S.; Helmann, J. D. A complex thiolate switch regulates the *Bacillus subtilis* organic peroxide sensor OhrR. *Proc. Natl. Acad. Sci. U. S. A.* **2007***, 104*, 8743-8748.

(48) Cho, S.; Lee, H. S.; Franzblau, S. Microplate alamar blue assay (MABA) and low oxygen recovery assay (LORA) for *Mycobacterium tuberculosis*. *Mycobacteria Protocols*. **2015**, *1285*, 281-292.

(49) (a) Basaraba, R. J.; Hunter, R. L. Pathology of Tuberculosis: How the pathology of human tuberculosis informs and directs animal models. *Microbiol. Spectr.* **2017***, 5*, 117-129. (b) Bloemberg, G. V.; Keller, P. M.; Stucki, D.; Trauner, A.; Borrell, S.; Latshang, T.; Coscolla, M.; Rothe, T.;

Hömke, R.; Ritter, C. Acquired resistance to bedaquiline and delamanid in therapy for tuberculosis. *N. Engl. J. Med.* **2015***, 373*, 1986-1988. (c) Ruesen, C.; Riza, A. L.; Florescu, A.; Chaidir, L.; Editoiu, C.; Aalders, N.; Nicolosu, D.; Grecu, V.; Ioana, M.; van Crevel, R. Linking minimum inhibitory concentrations to whole genome sequence-predicted drug resistance in *Mycobacterium tuberculosis* strains from Romania. *Scientific reports* **2018***, 8*, 9676.

(50) Makarov, V.; Manina, G.; Mikusova, K.; Mollmann, U.; Ryabova, O.; Saint-Joanis, B.; Dhar, N.; Pasca, M. R.; Buroni, S.; Lucarelli, A. P.; Milano, A.; De Rossi, E.; Belanova, M.; Bobovska, A.; Dianiskova, P.; Kordulakova, J.; Sala, C.; Fullam, E.; Schneider, P.; McKinney, J. D.; Brodin, P.; Christophe, T.; Waddell, S.; Butcher, P.; Albrethsen, J.; Rosenkrands, I.; Brosch, R.; Nandi, V.; Bharath, S.; Gaonkar, S.; Shandil, R. K.; Balasubramanian, V.; Balganesh, T.; Tyagi, S.; Grosset, J.; Riccardi, G.; Cole, S. T. Benzothiazinones kill *Mycobacterium tuberculosis* by blocking arabinan synthesis. *Science* **2009***, 324*, 801-804.

(51) Shirling, E. B.; Gottlieb, D. Methods for characterization of *Streptomyces* species. *Int. J. Syst. Evol. Microbiol.* **1966***, 16*, 313-340.

(52) Tamamura, T.; Sawa, T.; Isshiki, K.; Masuda, T.; Homma, Y.; Iinuma, H.; Naganawa, H.; Hamada, M.; Takeuchi, T.; Umezawa, H. Isolation and characterization of terpentecin, a new antitumor antibiotic. *J. Antibiot.* **1985***, 38*, 1664-1669.

(53) Madeira, F.; Lee, J.; Buso, N.; Gur, T.; Madhusoodanan, N.; Basutkar, P.; Tivey, A.; Potter, S. C.; Finn, R. D.; Lopez, R. The EMBL-EBI search and sequence analysis tools APIs in 2019. *Nucleic Acids Res.* **2019**, *47*, W636-W641.

(54) (a) Minowa, Y.; Araki, M.; Kanehisa, M. Comprehensive analysis of distinctive polyketide and nonribosomal peptide structural motifs encoded in microbial genomes. *J. Mol. Biol.* **2007***, 368*, 1500-1517. (b) Raushch, C.; Weber, T.; Kohlbacher, O.; Wohlleben, W.; Huson, D. H. Specificity prediction of adenylation domains in nonribosomal peptide synthetases (NRPS) using transductive support vector machines (TSVMs). *Nucl. Acids Res.* **2005***, 33*, 5799-5808.

(55) (a) Crooks, G. E.; Hon, G.; Chandonia, J. M.; Brenner, S. E. WebLogo: a sequence logo generator. *Genome Res.* **2004***, 14*, 1188-1190. (b) Schneider, T. D.; Stephens, R. M. Sequence logos: a new way to display consensus sequences. *Nucleic Acids Res.* **1990***, 18*, 6097-6100.

(56) Kieser, T. *Practical streptomyces genetics;* John Innes Foundation: 2000.

(57) Chen, C.; Wang, C.; Chu, C.; Su, L.; Chiu, C. Functional and molecular characterization of pSE34 encoding a type IV secretion system in *Salmonella enterica* serotype Enteritidis phage type 34. *FEMS Immunology & Medical Microbiology* **2009***, 57*, 274-283.

(58) Patterson, A. E.; Flewelling, A. J.; Clark, T. N.; Geier, S. J.; Vogels, C. M.; Masuda, J. D.; Gray, C. A.; Westcott, S. A. Antimicrobial and antimycobacterial activities of aliphatic amines derived from vanillin. *Canadian Journal of Chemistry* **2015***, 93*, 1305-1311.

(59) Overy, D. P.; Berrue, F.; Correa, H.; Hanif, N.; Hay, K.; Lanteigne, M.; Mquilian, K.; Duffy, S.; Boland, P.; Jagannathan, R.; Carr, G. S.; Vansteeland, M.; Kerr, R. K. Sea foam as a source of fungal inoculum for the isolation of biologically active natural products. *Mycology* **2014***, 5*, 130-144.

For table of contents only

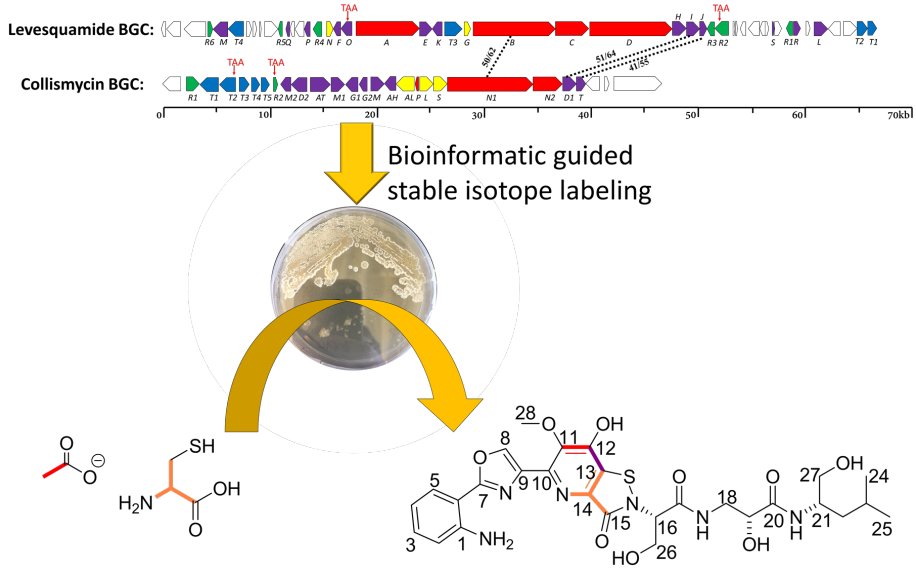

2020-05-04

Discovery of an isothiazolinone-containing antitubercular natural product Levesquamide

Liang, Libang

American Chemical Society

https://dx.doi.org/10.1021/acs.joc.0c00339